MJO teleconnections to crop growing seasons

Weston Anderson*

International Research Institute for Climate and Society, Palisades, New York

Ángel G. Muñoz, Lisa Goddard, Walter Baethgen, and Xandre Chourio

International Research Institute for Climate and Society, Palisades, New York

Corresponding author address: International Research Institute for Climate and Society, Palisades, New York

E-mail: weston@iri.columbia.edu

ABSTRACT

While many Madden-Julian Oscillation (MJO) teleconnections are well documented, the significance of these teleconnections to agriculture is not well understood. Here we analyze how the MJO affects the climate during crop flowering seasons, when crops are particularly vulnerable to abiotic stress. Because the MJO is located in the tropics of the summer hemisphere and maize is a tropical, summer-grown crop, the MJO teleconnections to maize flowering seasons are stronger and more coherent than those to wheat, which tends to be grown in midlatitudes and flowers during the spring.

The MJO significantly affects not only daily average precipitation and soil moisture, but also the probability of extreme precipitation, soil moisture and maximum temperatures during crop flowering seasons. The average influence on the probability of extreme daily precipitation, soil moisture, and maximum temperature events is roughly equal. On average the MJO modifies the probability of a 5th or 95th, 10th or 90th, and 25th or 75th percentile event by $\sim$2.5%, $\sim$4% and $\sim$7%, respectively. This means that an exceptionally dry (10th percentile) soil moisture value, for example, would become $\sim$40% more common (happening 14% of the time) during certain MJO phases.

That the MJO can simultaneously dry soils and raise maximum air temperatures may be particularly damaging to crops because without available soil water during times of heat stress, plants are unable to transpire to cool leaf-level temperatures as a means of avoiding long-term damage. As a result, even though teleconnections from the MJO last only a few days to a week, they likely affect crop growth.

1. Introduction

The Madden-Julian Oscillation (MJO) is a coupled ocean-atmosphere phenomena that, when it is active, organizes tropical atmospheric circulation at planetary scales into regions of enhanced and suppressed convection. It is the dominant source of subseasonal climate variability in the tropics, accounting for ∼40-50% of tropical outgoing longwave radiation (OLR) variance (Kessler 2001), although the intensity and duration of MJO activity varies from year-to-year.

MJO-related anomalies propagate eastward with a phase speed of ~ 5 m/s, which gives the oscillation a period of 30-60 days (see review by Zhang (2005)). Deep convective anomalies associated with the MJO often first appear over the Indian Ocean and reach the western Pacific about two weeks later. The surface expression of the MJO dissipates as it propagates eastward over the cold sea surface temperatures in the eastern Pacific before reforming in the tropical Atlantic. Although the MJO may be active in all seasons, the meridional location of the primary convective envelope tends to follow the migration of the Inter-Tropical Convergence Zone (ITCZ) such that MJO activity is displaced into the summer hemisphere by 5-10 degrees (Zhang and Dong 2004).

The influence of the MJO is not confined to the tropics. It has widespread teleconnections that affect the climate of both the subtropics and the midlatitudes. The MJO has been shown to influence the Asian (Lawrence and Webster 2002), Australian (Wheeler et al. 2009), West African (Lavender and Matthews 2009; Matthews 2004; Barlow 2012), and Indian monsoons (Joseph et al. 2009; Pai et al. 2011), as well as the rainy seasons in East Africa (Pohl and Camberlin 2006a,b; Berhane and Zaitchik 2014), southwest Asia (Barlow et al. 2005; Nazemosadat and Ghaedamini 2010; Barlow 2012), and southern Mexico (Barlow and Salstein 2006). In the midlatitudes a less strong and possibly seasonally dependent influence has been found in the United States (Bond and Vecchi 2003; Zhou et al. 2012), South Africa (Pohl et al. 2007), and Southeast South America

(Grimm 2019; Alvarez et al. 2016). The MJO has also been shown to affect the probability of extreme precipitation (Barlow et al. 2005; Muñoz et al. 2015) and maximum temperatures (Lee and Grotjahn 2019).

Despite the extensive research on the connection between the MJO and climate anomalies, there has been no effort yet to analyze how the MJO affects agriculture through its spatio-temporal teleconnections. That the MJO is an intraseasonal rather than seasonal mode of variability may complicate such analyses, but it does not indicate that the MJO is any less able to influence crop yields. There is significant evidence that daily-scale abiotic stresses can appreciably affect final crop yields (Schlenker and Roberts 2009; Lesk et al. 2016), particularly when crops have inadequate access to available soil moisture (De Boeck et al. 2011; Amani et al. 1996; Troy et al. 2015). Even a single day of exposure to damaging maximum temperatures can lower final crop yields (Schlenker and Roberts 2009), and the MJO tends to persist in each of its 8 phases for 3-7 days (Pohl and Matthews 2007). If the MJO influences agriculturally relevant variables, such as soil moisture and damaging maximum temperatures, during relevant periods of the crop growing season, then it is likely to also affect crop yields.

In this article we outline the ways in which the MJO affects crop-relevant variables during local wheat and maize growing seasons. In particular, we focus on the reproductive period of the crop growing season because that is when grain crops are most sensitive to climate stresses (Barnabás et al. 2008). Section two outlines the data and methods. Section three discusses the global structure and strength of MJO teleconnections relative to local crop growing seasons before moving into a region-by-region description of each teleconnection. Results for both the strength of MJO teleconnections, and the influence of the MJO on the probability of extreme precipitation, soil moisture, and damaging maximum temperature anomalies are presented.

2. Data and Methods

a. Agricultural data

To identify agricultural areas, we use harvested area data for wheat and maize around the year 2000 (Ramankutty et al. 2008; Monfreda et al. 2008). Although there are more recent datasets, such as the harvested area dataset from the International food policy research institute (IFPRI) for 2005 (IFPRI and IIASA 2016) and 2010 (IFPRI 2019), we use cropped area in only an illustrative context to highlight cropped regions. Global data for crop growing seasons is taken from Sacks et al. (2010), and flowering season are approximated as being the three months preceding harvest of each crop. We focus on crop flowering because it is the time when grain crops are most sensitive to abiotic stresses (Barnabás et al. 2008). While in reality crops will be harvested earlier or later depending on the year, limited data availability forces us to assume a static cropping calendar. We use a combination of growing regions for each crop and past literature on MJO teleconnections to choose the regions that we analyze.

b. MJO event identification

To identify MJO events we use the Wheeler-Hendon Realtime Multivariate MJO (RMM) index Wheeler and Hendon (2004). The RMM indices (RMM1 and RMM2) are derived as a pair of multi-variate empirical orthogonal functions of OLR, 850-hPa zonal winds, and 200-hPa zonal winds. Projection of observations onto these indices measures the intensity and location of atmospheric circulation and precipitation patterns associated with the MJO.

We define MJO events during crop flowering seasons as those days in which the amplitude of the RMM index exceeds one standard deviation. We then create composites or distributions based on all identified days. We mask out all gridboxes in which there are fewer than 1000 observations or

where either maize or wheat is not cultivated. We furthermore test whether the distribution of each variable at each point during a given phase is statistically distinguishable from the distribution of that variable when the MJO is in its neutral phase (having an amplitude less than one). We mask areas where the distribution is not significantly different at the 5% level.

c. Climate data

To identify MJO teleconnections we use daily-scale atmospheric variables from reanalyses, interpolated station-based data, and products that integrate both satellite and station data using statistical or physicaly-based models. For data on geopotential height and vertically integrated moisture flux we use ECMWF six hourly ERA-Interim values aggregated to a daily resolution (Dee et al. 2011). We standardize the geopotential height data by removing the mean and dividing by the standard deviation at each point. For outgoing longwave radiation (OLR) we use gridded daily data from the National Oceanic and Atmospheric Administration (NOAA) with temporal interpolation (Liebmann and Smith 1996). Velocity potential was not available in the ERA Interim reanalysis, but was available as a derived variable from the NCEP/NCAR Reanalysis I (Kalnay et al. 1996) via `http://apdrc.soest.hawaii.edu/datadoc/ncep_daily.php`. For information on soil moisture, we use daily surface (0-10cm) soil moisture estimates from the Global Land Evaporation Amsterdam Model (GLEAM) v3.2a, which uses satellite-observed soil moisture, vegetation optical depth, reanalysis air-temperatures and a multi-source precipitation product to derive surface and root-zone soil moisture values (Martens et al. 2017). Daily precipitation data comes from the Climate Hazards group Infrared Precipitation with Stations (CHIRPS) at 0.25 degrees (Funk et al. 2015). To estimate temperatures that would be damaging to crops, we use values of daily maximum temperature at 2m from the Berkeley Earth dataset, which is a 1 degree gridded interpolation-based statistical product (Rohde et al. 2013).

While all datasets are observationally constrained, there remain significant limitations to each. We expect that the temperature and precipitation data will be of higher quality in regions with extensive gauge-based records as compared to more data scarce regions in which statistical extrapolation or satellite-based measurements are the main source of information. Owing to a lack of soil moisture gauge station data globally, GLEAM soil moisture estimates rely on a simple water balance model constrained by assimilation of microwave satellite-based estimates, which are limited to measuring the top few centimeters of the soil, and reanalysis-based soil moisture estimates. GLEAM produces a best-guess observational constraint from the satellite and reanalysis datasets using triple collocation analysis, an approach that has shown promise previously in data-sparse regions (Anderson et al. 2012).

d. Daily climate anomalies

To estimate the impact of harmful increases in maximum temperature around flowering, we follow the methods of Schlenker and Roberts (2009) by using critical temperature thresholds (T_c) for wheat and maize as 26°C and 29°C, respectively. Our temperature thresholds are chosen to identify detrimental, not necessarily lethal, temperatures (Sánchez et al. 2014). During the three months around flowering, the number of 'extreme degree days' (EDD) were then calculated as follows:

$$EDD = \sum_{i=1}^{n} max(0, T_{max,i} - T_c)$$

where $T_{max,i}$ is the maximum temperature on the ith day of the flowering period (that lasts n days). We use an average of daily EDDs across all years to define the climatology of EDDs.

For atmospheric anomalies – geopotential height, vertically integrated moisture flux, vertical velocity potential, and outgoing longwave radiation (OLR) – we similarly calculate daily anomalies as the departures from an average across all years for the same day. For precipitation and near-

surface soil moisture, which are potentially noisy variables, we first compute the average across all years for the same day to define the daily climatology. We then perform a Fourier analysis on the daily climatology using fast Fourier transforms and retaining only the first three harmonics to calculate the smoothed daily climatology.

e. Probabilistic teleconnections

To calculate the 5%, 10%, 25%, 75%, 90% and 95% event thresholds we rank all precipitation, soil moisture and EDD anomalies during the days when the MJO is inactive, then identify the magnitude of the anomaly corresponding to each percentile. For each MJO phase we then count the number of events that exceed that intensity threshold to calculate the frequency of events that are at least that extreme. The anomalous probability of exceeding the 90th percentile for daily precipitation during MJO phase 8, for example, would be calculated as:

$$\delta P(Pr > Pr_{90}|MJO_8) = P(Pr > Pr_{90}|MJO_8) - P(Pr > Pr_{90}|MJO_{neutral}) \quad (1)$$

Where Pr_{90} is the event that marks the 90th percentile, Pr is daily precipitation, MJO_8 indicates days when the MJO has an amplitude greater than one and is in phase 8, and $MJO_{neutral}$ indicates MJO with amplitude less than one.

f. Significance testing

We apply two types of significance testing in our analysis, one significance test that accounts for testing many points in space simultaneously, and one for testing the significance of shifts in the probability of exceeding a quantile threshold (e.g. 5th, 10th, 25th percentile). When we test for significant MJO teleconnections in the global domain, we are testing a great number of points and would expect to get a number of false positives because each grid point constitutes an individual statistical test. We control the false discovery rate by following the methods of Wilks (2016), which

includes a correction for spatial auto-correlation in climate data. Each grid point must pass the field significance criteria to be considered statistically significant. For assessing the significance of changes in the frequency of extreme events in a region, we apply the hypergeometric test, which measures whether a sample distribution (in this case the days in a particular MJO phase) has an inflated or deflated frequency of event occurrences (e.g. days with extreme precipitation) compared to the reference distribution. Both significance tests are applied at the 95% confidence level.

3. Results

a. Global teleconnections to wheat and maize growing seasons

Whether or not the MJO affects agriculture will depend on the intersection of (1) the seasonality of MJO activity and (2) the timing of crop growing seasons. The MJO follows the seasonal migration of the Inter-Tropical Convergence Zone (ITCZ) such that precipitation and wind variance associated with the MJO tend to be centered in the summer hemisphere by about 10 degrees (e.g. 10N in boreal summer, 10S in austral summer; Zhang and Dong (2004)). This tendency is reflected in OLR (Figs. 1 and 2) and moisture flux composites (Figs. 12 and 13), which are similarly displaced into the summer hemisphere.

The crop reproductive period, when grain crops are most sensitive to abiotic climate stresses (Barnabás et al. 2008), occurs in the months prior to harvest; maize flowers during local summer while wheat flowers in local spring. Because the MJO is displaced into the summer hemisphere, and the most sensitive period of the maize lifecycle occurs during summer, one may anticipate that the MJO will strongly affect summer-flowering crops like maize.

In addition to seasonality, however, the location of MJO teleconnections relative to crop growing locations is important. The majority of anomalous convection and moisture fluxes associated with the MJO are confined to the tropics (roughly 20N/S; see Figs 1 - 13; see also Zhang and Dong (2004)), although there are teleconnections outside of these latitudes as well. These MJO-forced anomalies will overlap with maize growing regions more frequently than with wheat growing regions because maize is grown in the tropics while wheat is often grown in the midlatitudes (Figs. 3 and 4).

The seasonality and location of crops and that of the MJO explain why the MJO has a stronger, more coherent effect on maize flowering seasons as compared to wheat flowering seasons. Because maize is often grown in the summer hemisphere near the equator, the MJO has a coherent influence on over a dozen independent maize seasons globally (Fig. 3). The magnitude of the MJO influence often reaches 20-40% of expected daily precipitation during the maize flowering season. Because wheat is not a summer crop, and is often grown in the midlatitudes, the MJO influence on wheat flowering seasons is more location-dependent. MJO teleconnections to wheat flowering seasons in the tropics and subtropics – Southwest Asia, India and East Africa – tend to be stronger and more coherent compared to those in the midlatitudes – Southeast South America, The United States, Australia, South Africa, and the North China Plain (Fig. 4)

The MJO affects both precipitation and soil moisture during the wheat and maize growing seasons, although it tends to influence precipitation more strongly than soil moisture compared to a day with neutral conditions (Figs. 3 and 4). For both wheat and maize, the strength of MJO teleconnections to soil moisture during the growing season tends to be a 2.5-5% modification of a climatological value (5-10% difference from positive to negative phase), although local modifications can be over 10% (20% difference between positive and negative phases). The influence of the

MJO on precipitation in many regions exceeds 25% (50% difference between phases) and in some regions, such as East Africa, its influence can exceed 50% (100% difference between phases).

The MJO modifies the probability of extreme events at least as strongly as it does the probability of moderate events. The MJO increases the relative probability of a 5th percentile event by 50% (e.g., an event that normally happens 5% of the time instead occurs 7.5% of the time), of a 10th percentile event by 30% (10% event becomes 13% event) and of a 25th percentile event by 20% (25% event becomes 30% event) during both maize and wheat flowering seasons (Figs. 5 - 10). Furthermore, the MJO affects the probability of dry events (5, 10 and 25%) more strongly than it does wet events (95, 90, 75%), particularly during the maize flowering season. This is consistent with observations made by Pohl et al. (2009) for the Sahel and West Africa.

b. Regional analyses

1) AFRICA

In East Africa, the MJO affects precipitation differently in the highlands and the coast. In the highlands precipitation anomalies are controlled by the large-scale atmospheric stability conditions imposed by the MJO, while near the coast advection of moisture by local low-level winds dominates (Pohl and Camberlin 2006a,b; Berhane and Zaitchik 2014; Barlow 2012). In the highlands around Lake Victoria, phases 6-8 tend to lead to suppressed convection (Fig 2 and 3), which decreases soil moisture and increases the probability of extremely hot temperatures during phases 7-1 (Figs. 6 and 7). The teleconnections to the wheat growing highlands in Ethiopia are similar to those in the highlands of Kenya, with the exception that in Ethiopia teleconnections to extreme precipitation are often not significant. While no detailed analysis on the dynamics of MJO teleconnections to the Ethiopian highlands was available, it is likely that the MJO teleconnections will be dominated by large-scale atmospheric stability as they are elsewhere in the highlands of East

Africa (Pohl and Camberlin 2006a; Berhane and Zaitchik 2014). The moisture teleconnections in coastal East Africa - here the focus is on southern Somalia - are instead related to moisture transport into/out of the region (Figs. 12-13; see also Pohl and Camberlin (2006a) for the MAM and OND seasons)

Southern Africa, although largely outside of the main convective envelope of the MJO, has significant teleconnections to crop growing seasons. Increased convection first shows up over Namibia in western South Africa during phases 5-6 and propagates south and east into northeast South Africa in phases 6-7 before increased convection arrives over Mozambique and Malawi in phases 1-3 (see Figs. 1, 3 and 4; Pohl et al. (2007)). Phases 6-1 of the MJO tend to be wet (Figs. 3-4) and to decrease the probability of extremely hot conditions during the wheat flowering season (Fig. 10). Wet phases over Northeast South Africa (phases 6-1) are associated with a reinforcement of climatological easterly and northerly moisture fluxes from the Western Indian Ocean and Zambia/Botswana/Zimbabwe into South Africa (Figs. 12 and 13).

In West Africa, the MJO increases the probability of wet conditions in phases 1-3 and of dry conditions in phases 5-7. Soil moisture teleconnections tend to lag precipitation teleconnections by one phase, as do teleconnections to maximum temperature (Fig. 3, 5-7). These teleconnections are primarily a response to westward propagating Rossby waves generated by MJO-related convection $\sim$10 days earlier (Lavender and Matthews 2009; Matthews 2004; Barlow 2012). When the MJO suppresses convection in the warm pool (phases 7-2; see Figs. 1 and 2), it generates Rossby waves that travel west and an equatorial Kelvin wave that travels east (visible in lower-level GPH anomalies, Figs. 12 and 13). The westward propagating Rossby wave moves across West Africa 5-10 days after being generated, destabilizes the atmospheric column and enhance rainfall in the region (Lavender and Matthews 2009; Matthews 2004). The reverse is true 5-10 days after phase 3-6. Because the MJO propagates eastward, these lagged responses may alias onto composites of

MJO temperature and precipitation anomalies (Vigaud and Giannini 2018). The wet conditions in phases 1-3 are, therefore, a lagged response to convection over the warm pool in phases 7-2.

2) ASIA

The MJO has strong teleconnections to wheat growing season precipitation and soil moisture in Southwest Asia, and less strong but still at times significant teleconnections to the Fertile Crescent (Fig. 4). On average, suppressed convection over the eastern Indian Ocean during phases 8-1 (see Figs. 1 and 2) leads to an increase of precipitation over Southwest Asia (Fig. 4 and Barlow et al. (2005); Barlow (2012)). The opposite is true in phases 4-5. MJO teleconnections affect not only the mean precipitation in Southwest Asia, but also precipitation frequency (Nazemosadat and Ghaedamini 2010) and extremes (Barlow et al. 2005). During phases 4-6 the MJO increases the probability that a day in Southwest Asia will be extremely dry, while phases 8-2 increase the probability of an extremely wet day (Figs. 8)-9). Soil moisture teleconnections tend to lag precipitation teleconnections by about one phase (Fig. 4). Maximum temperature teleconnections in both regions are mostly not statistically significant (Fig. 10).

In India the MJO affects precipitation and soil moisture during both the maize and wheat growing season in major growing areas (Figs. 3 and 4). It is worth noting that the strength of MJO teleconnections in Figures 3 and 4 are expressed as a percent of average daily precipitation during the growing season – not precipitation on rainy days – and that maize is grown during the monsoon season while wheat is grown during the dry season. So although the MJO has a weaker absolute effect on Indian precipitation during the wheat growing season (Figs. 1 amd 2), the effect is still significant in the context of dry-season rainfall and soil moisture (Fig. 4).

The eastward propagating deep convection anomalies associated with the MJO generate meridionally-propagating Rossby waves that modify precipitation over India in the 10-25N region

up to two weeks later (Lawrence and Webster 2002). The longest monsoon breaks are associated with times when the MJO suppresses convection over the Indian Ocean (Joseph et al. 2009; Moron et al. 2012). An increased frequency of MJO phases 7-2 are associated with long monsoon breaks, although the longest breaks are associated with phase 7 (Pai et al. 2011). These past analyses are consistent with our OLR composites during the monsoon season (Figs. 1 and 2) that show increased OLR during phases 7-2, which is an indication of decreased precipitation (Fig. 3) that, with a one to two phase lag, leads to decreased near-surface soil moisture and increased maximum temperatures. The lag between precipitation and maximum temperature – likely a result of the time needed for the soil to dry out and force a shift in the partitioning of latent to sensible heat – accounts for why the frequency of extreme temperatures are increased during phases 1-3 rather than 7-2. During phases 4-5 OLR decreases, precipitation increases, soil moisture increases, and maximum temperatures decrease (Figs. 3 and 5-7). During the dry wheat season, the MJO decreases the probability of moderate to exceptionally wet days in phases 4-6 and increases the probability of exceptionally dry soil moisture and hot temperatures (Figs. 4 and 8-10).

In the North China Plain, MJO phase 2 has increased precipitation, while phases 7-1 tend to be dry (Figs. 4). Soil moisture teleconnections persist for 1-2 phases after precipitation teleconnections (Figs. 4 and 8-9). Moisture transports into and out of the North China Plain may be related to the Rossby wave north of the convective center of the MJO (Figs. 1-13) but a proper moisture budget analysis is beyond the scope of this paper. Provided the agricultural importance of the North China Plain, further research on boreal springtime MJO teleconnections to this region is needed.

3) AUSTRALIA AND THE MARITIME CONTINENT

Over the Maritime Continent, OLR becomes a less good proxy for precipitation because large-scale atmospheric conditions may differ from the localized dynamics that govern precipitation over land. Precipitation anomalies over land tend to lead the eastward-propagating of OLR anomalies by $\sim$6 days, such that large scale atmospheric conditions can be unfavorable to precipitation over the ocean but precipitation over land in Indonesia will be enhanced (compare Figs. 1 and 2 to Fig. 5; Peatman et al. (2014)).

During the maize flowering seasons, MJO phases 2-4 tend to be wet and cool, while phases 6-8 tend to be dry (Figs 6 and 5 - 7). Our results for June to September (Figs. 1, 2 and 6) lead those of Moron et al. (2015), who found that during the September-April season phases 1-3 tend be wet and phases 5-7 tend to be dry. This discrepancy highlights that MJO teleconnections have a degree of seasonal variability, and that analyses conducted using different seasons may not be directly applicable to the growing season.

During the wheat growing season in Australia, the MJO affects mean precipitation and both mean and extreme soil moistures and temperatures. Wheeler et al. (2009) find that in extratropical Southeast Australia, the MJO both modifies large-scale ascent/descent and moisture transport via low-level meridional winds. The MJO increases moisture transport into Southeast Australia during phases 5-7 and increases moisture transport out of the region in phases 8-2 (Figs. 1 and 2; Wheeler et al. (2009)). This leads to increased precipitation during phase 5, which increases soil moisture in phases 5-7, and decreases precipitation during phases 1-2, which decreases soil moisture during phases 1-3 (Fig. 4). The MJO affects growing season extremes as well by increasing the probability of extremely dry soil moisture days and damaging extreme temperatures during

phases 1-3 (Figs 6 and 7). The opposite effect of the MJO on extremely wet, cool, days is less pronounced.

4) North and Central America

The MJO affects precipitation, soil moisture and maximum temperatures during the maize flowering season across Southern Mexico and Central America. In phases 8-2 convection is enhanced while convection is suppressed during phases 4-6 (Figs. 1, 2 and 3). This strong MJO teleconnection is clearly visible during boreal summer (JJAS) but not in austral summer (DJFM; Figs. 12 and 13). Barlow and Salstein (2006) conclude from gauge station data that the precipitation signal is strongest on the western side of the continent as a result of westerly moisture flows and orography. During phases 8-2 westerly winds advect moisture onshore (Figs. 12 and 13), where steep topography induces precipitation and increases soil moisture (Fig. 3). These same conditions bring opposite conditions to the eastern side of southern Mexico and Central America.

The MJO also affects the frequency of extremely dry, hot days in Mexico and Central America. During phases 3-6 the probability of days with extremely low precipitation, low soil moisture and hot temperatures increases while the probability of wet, cool days decreases (Figs. 5-7). Phases 8-2 exhibit an increased number of cool, wet days and decrease in the frequency of dry, hot days, although the effect is more muted than during phases 3-5

The MJO has previously been found to affect precipitation over the Pacific Northwest with a phasing that is seasonally dependent (Bond and Vecchi 2003). In agreement with Bond and Vecchi (2003), we find that mean precipitation in the Pacific Northwest increases (Fig 4) when deep convection is suppressed in the eastern Indian Ocean (Figs. 1 and 2) and there are westerlies near the date line (Figs. 12 and 13). However, when considering specific quantiles of precipitation, the results are either not statistically significant or are inconsistent with the MJO uniformly shifting

the distribution of precipitation towards wetter or drier anomalies. In either case, it appears that teleconnections to the region are not easily generalizable for the context of agriculture.

MJO teleconnections to wheat flowering seasons in the Great Plains are weak and only marginally significant. The MJO tends to make the southern Great Plains dry during wheat flowering seasons in phases 4-6 and wet during phase 2, but has an inconsistent or insignificant effect during most other phases (Figs 4, 8-10). Our results for springtime precipitation teleconnections differ from those of Zhou et al. (2012), who focus on winter precipitation teleconnections and find that phases 5-6 tend to be wet.

5) South America

The MJO affects the maize growing seasons in Western South America, with phases 8-2 favoring wet conditions while phases 3-7 tend to be dry (Fig. 3). An increased probability of extremely high precipitation, high soil moisture and low maximum temperatures accompanies the wet conditions in phases 1-2, while extremely low soil moisture, low precipitation are more frequent in phases 3-7 (Figs. 5-6). Furthermore, phases 3-4 are associated with an increase in the frequency of extremely hot, damaging temperatures (Fig. 7)

Over Northeast Brazil OLR and atmospheric descent is increased during phases 4-6 (Figs. 1 and 2), which translates into reduced precipitation, decreased near-surface soil moisture (Fig 3), and an increased probability of damaging maximum temperatures (Fig 7). During these phases Northeast Brazil is more likely to experience extremely dry conditions, and less likely to have exceptionally wet days as measured by both precipitation and soil moisture (Figs. 5 and 6). During phases 8-2 OLR is decreased over Northeast Brazil (Figs. 1 and 2), indicating an increase in precipitation (Fig. 3). In these phases the frequency of exceptionally wet days is enhanced – particularly in phase 8 – and the probability of extremely hot conditions decreases (Figs. 5-7). These results are

consistent with those of (Valadão et al. 2017; Alvarez et al. 2016), who use station data and gridded station data, respectively, to demonstrate the seasonality of MJO teleconnections to precipitation in South America.

Similar to Northeast Brazil, central eastern South America tends to be wetter during phases 8-2 and drier during phases 3-7 (Fig 3) with extremely wet, cool days occurring more frequently in phases 8-2 and extremely hot, dry days occurring more frequently in phases 3-6 (Figs. 5-7). These findings are consistent with those of Grimm (2019), who uses gridded station data to measure the effects of the MJO on average and extreme precipitation events. The asymmetric influence of the MJO in central eastern South America (e.g. five phases favor dry anomalies while only three favor wet anomalies) is also consistent with the findings of Grimm (2019).

In Southeast South America, the MJO forces wet conditions during phases 3-6 and dry, hot conditions during phase 8 in southeastern South America during austral summer, the maize growing season (Figs. 3, 5 - 7; see also Grimm (2019) and Muñoz et al. (2015, 2016)). The MJO, however, has little coherent influence on extreme temperatures aside from phase 8 (Fig 7).

4. Discussion

Our analysis demonstrates that the MJO affects not only precipitation, but also soil moisture and damaging maximum temperatures – those that exceed 26°C for wheat or 29°C for maize – during local crop flowering seasons (see Figure 11 for a summary). That the MJO simultaneously drys the soil and increases maximum air temperatures is particularly relevant to crops because without available soil water during times of heat stress, crops are unable to transpire to cool leaf-level temperatures as a means of avoiding long-term damage. Even a single day spent exposed to extreme heat can significantly lower the final yield of a crop (Schlenker and Roberts 2009). So although MJO teleconnections may last only a few days to a week, they may affect crop yields.

The MJO affects both wheat and maize flowering seasons, but it more strongly affects maize flowering seasons than wheat flowering seasons. The MJO is preferentially located in the tropics of the summer hemisphere and maize is a tropical, summer-grown crop. The MJO teleconnections to maize regions during flowering seasons are therefore stronger and more coherent than those to wheat, which tends to be grown in midlatitudes and flowers during the spring. These findings may extend beyond the comparison of maize to wheat. Due to the seasonal, latitudinal migration of convection associated with the MJO, it is likely to more strongly affect the growing conditions of tropical and sub-tropical, summer crops as compared to those grown in other seasons or in other regions, although further research is needed to confirm this.

Of particular relevance to crop yields is the finding that the MJO affects climate extremes during the crop flowering season. The average influence on extreme daily precipitation, soil moisture, and maximum temperature events is roughly equal. On average the MJO modifies the probability of a 5th (95th), 10th (90th), and 25th (75th) percentile event by 2.5%, 4% and 7%, respectively. This means that an exceptionally dry (10th percentile) soil moisture value, for example, would become $\sim$40% more common (happening 14% of the time) during certain MJO phases.

Our results provide an indication of the extent to which the MJO affects global crop growing seasons, and the mechanisms by which it does so. With the development of seasonal-to-subseasonal (S2S) forecasting (White et al. 2017; Vitart and Robertson 2018), there is increasing evidence that climate anomalies associated with the MJO may be predictable at lead times of 3-4 weeks in some regions (DelSole et al. 2017; Pegion et al. 2019). But the lack of sector-specific studies complicates the process of integrating S2S forecasts into an operational setting (Vitart and Robertson 2018). Our results can serve as a guide for improving model forecasts of subseasonal predictions for the agriculture sector.

5. Appendix A

Figurers 12 and 13 are composites of atmospheric MJO teleconnections to standardized geopotential height and total column moisture transport in each phase. These figures provide context when assessing how MJO teleconnections lead to anomalous precipitation and temperature during crop growing conditions.

Acknowledgments. This project was supported by ACToday, a Columbia World Project. A. Muñoz was partially supported by the NOAA award NA18OAR4310275. W. Anderson acknowledges support from the Earth Institute at Columbia University. The authors would like to thank Kátia Fernandes for helpful discussions on the MJO in Northeast Brazil, Simon Mason for discussions about statistics of daily anomalies and statistical significance, Zane Martin for the helpful discussions on our analysis, and Michael Bell for help with the IRI Data Library code.

References

Alvarez, M. S., C. S. Vera, G. N. Kiladis, and B. Liebmann, 2016: Influence of the madden julian oscillation on precipitation and surface air temperature in south america. *Climate dynamics*, **46 (1-2)**, 245–262.

Amani, I., R. Fischer, and M. Reynolds, 1996: Canopy temperature depression association with yield of irrigated spring wheat cultivars in a hot climate. *Journal of Agronomy and Crop Science*, **176 (2)**, 119–129.

Anderson, W., B. Zaitchik, C. Hain, M. Anderson, M. Yilmaz, J. Mecikalski, and L. Schultz, 2012: Towards an integrated soil moisture drought monitor for east africa. *Hydrology and Earth System Sciences*, **16 (8)**, 2893–2913.

Barlow, M., 2012: Africa and west asia. intraseasonal variability in the atmosphere-ocean climate system, wk-m. lau and de waliser, eds. Springer.

Barlow, M., and D. Salstein, 2006: Summertime influence of the madden-julian oscillation on daily rainfall over mexico and central america. *Geophysical research letters*, **33 (21)**.

Barlow, M., M. Wheeler, B. Lyon, and H. Cullen, 2005: Modulation of daily precipitation over southwest asia by the madden–julian oscillation. *Monthly weather review*, **133 (12)**, 3579–3594.

Barnabás, B., K. Jäger, and A. Fehér, 2008: The effect of drought and heat stress on reproductive processes in cereals. *Plant, cell & environment*, **31 (1)**, 11–38.

Berhane, F., and B. Zaitchik, 2014: Modulation of daily precipitation over east africa by the madden–julian oscillation. *Journal of Climate*, **27 (15)**, 6016–6034.

Bond, N. A., and G. A. Vecchi, 2003: The influence of the madden–julian oscillation on precipitation in oregon and washington. *Weather and Forecasting*, **18 (4)**, 600–613.

De Boeck, H. J., F. E. Dreesen, I. A. Janssens, and I. Nijs, 2011: Whole-system responses of experimental plant communities to climate extremes imposed in different seasons. *New Phytologist*, **189 (3)**, 806–817.

Dee, D. P., and Coauthors, 2011: The era-interim reanalysis: Configuration and performance of the data assimilation system. *Quarterly Journal of the royal meteorological society*, **137 (656)**, 553–597.

DelSole, T., L. Trenary, M. K. Tippett, and K. Pegion, 2017: Predictability of week-3–4 average temperature and precipitation over the contiguous united states. *Journal of Climate*, **30 (10)**, 3499–3512.

Funk, C., and Coauthors, 2015: The climate hazards infrared precipitation with stations—a new environmental record for monitoring extremes. *Scientific data*, **2**, 150 066.

Grimm, A. M., 2019: Madden–julian oscillation impacts on south american summer monsoon season: precipitation anomalies, extreme events, teleconnections, and role in the mjo cycle. *Climate Dynamics*, 1–26.

IFPRI, 2019: *Global Spatially-Disaggregated Crop Production Statistics Data for 2010 Version 1.0*. https://doi.org/10.7910/DVN/PRFF8V, International Food Policy Research Institute.

IFPRI, and IIASA, 2016: *Global Spatially-Disaggregated Crop Production Statistics Data for 2005 Version 3.2*. https://doi.org/10.7910/DVN/DHXBJX, International Food Policy Research Institute (IFPRI); International Institute for Applied Systems Analysis (IIASA).

Joseph, S., A. Sahai, and B. Goswami, 2009: Eastward propagating mjo during boreal summer and indian monsoon droughts. *Climate Dynamics*, **32 (7-8)**, 1139–1153.

Kalnay, E., and Coauthors, 1996: The ncep/ncar 40-year reanalysis project. *Bulletin of the American meteorological Society*, **77 (3)**, 437–472.

Kessler, W. S., 2001: Eof representations of the madden–julian oscillation and its connection with enso. *Journal of Climate*, **14 (13)**, 3055–3061.

Lavender, S. L., and A. J. Matthews, 2009: Response of the west african monsoon to the madden–julian oscillation. *Journal of Climate*, **22 (15)**, 4097–4116.

Lawrence, D. M., and P. J. Webster, 2002: The boreal summer intraseasonal oscillation: Relationship between northward and eastward movement of convection. *Journal of the atmospheric sciences*, **59 (9)**, 1593–1606.

Lee, Y.-Y., and R. Grotjahn, 2019: Evidence of specific mjo phase occurrence with summertime california central valley extreme hot weather. *Advances in Atmospheric Sciences*, **36 (6)**, 589–602.

Lesk, C., P. Rowhani, and N. Ramankutty, 2016: Influence of extreme weather disasters on global crop production. *Nature*, **529 (7584)**, 84.

Liebmann, B., and C. A. Smith, 1996: Description of a complete (interpolated) outgoing longwave radiation dataset. *Bulletin of the American Meteorological Society*, **77 (6)**, 1275–1277.

Martens, B., and Coauthors, 2017: Gleam v3: Satellite-based land evaporation and root-zone soil moisture. *Geoscientific Model Development*, **10 (5)**, 1903–1925.

Matthews, A. J., 2004: Intraseasonal variability over tropical africa during northern summer. *Journal of Climate*, **17 (12)**, 2427–2440.

Monfreda, C., N. Ramankutty, and J. A. Foley, 2008: Farming the planet: 2. geographic distribution of crop areas, yields, physiological types, and net primary production in the year 2000. *Global biogeochemical cycles*, **22 (1)**.

Moron, V., A. W. Robertson, and M. Ghil, 2012: Impact of the modulated annual cycle and intraseasonal oscillation on daily-to-interannual rainfall variability across monsoonal india. *Climate dynamics*, **38 (11-12)**, 2409–2435.

Moron, V., A. W. Robertson, J.-H. Qian, and M. Ghil, 2015: Weather types across the maritime continent: from the diurnal cycle to interannual variations. *Frontiers in Environmental Science*, **2**, 65.

Muñoz, Á., L. Goddard, S. Mason, and A. Robertson, 2016: Cross–time scale interactions and rainfall extreme events in southeastern south america for the austral summer. part ii: Predictive skill. *Journal of Climate*, **29 (16)**, 5915–5934.

Muñoz, Á. G., L. Goddard, A. W. Robertson, Y. Kushnir, and W. Baethgen, 2015: Cross–time scale interactions and rainfall extreme events in southeastern south america for the austral summer. part i: Potential predictors. *Journal of Climate*, **28 (19)**, 7894–7913.

Nazemosadat, M., and H. Ghaedamini, 2010: On the relationships between the madden–julian oscillation and precipitation variability in southern iran and the arabian peninsula: Atmospheric circulation analysis. *Journal of Climate*, **23 (4)**, 887–904.

Pai, D., J. Bhate, O. Sreejith, and H. Hatwar, 2011: Impact of mjo on the intraseasonal variation of summer monsoon rainfall over india. *Climate Dynamics*, **36 (1-2)**, 41–55.

Peatman, S. C., A. J. Matthews, and D. P. Stevens, 2014: Propagation of the madden–julian oscillation through the maritime continent and scale interaction with the diurnal cycle of precipitation. *Quarterly Journal of the Royal Meteorological Society*, **140 (680)**, 814–825.

Pegion, K., and Coauthors, 2019: The subseasonal experiment (subx): A multi-model subseasonal prediction experiment. *Bulletin of the American Meteorological Society*, **(2019)**.

Pohl, B., and P. Camberlin, 2006a: Influence of the madden–julian oscillation on east african rainfall. i: Intraseasonal variability and regional dependency. *Quarterly Journal of the Royal Meteorological Society*, **132 (621)**, 2521–2539.

Pohl, B., and P. Camberlin, 2006b: Influence of the madden–julian oscillation on east african rainfall: Ii. march–may season extremes and interannual variability. *Quarterly Journal of the Royal Meteorological Society*, **132 (621)**, 2541–2558.

Pohl, B., S. Janicot, B. Fontaine, and R. Marteau, 2009: Implication of the madden–julian oscillation in the 40-day variability of the west african monsoon. *Journal of Climate*, **22 (13)**, 3769–3785.

Pohl, B., and A. J. Matthews, 2007: Observed changes in the lifetime and amplitude of the madden–julian oscillation associated with interannual enso sea surface temperature anomalies. *Journal of Climate*, **20 (11)**, 2659–2674.

Pohl, B., Y. Richard, and N. Fauchereau, 2007: Influence of the madden–julian oscillation on southern african summer rainfall. *Journal of Climate*, **20 (16)**, 4227–4242.

Ramankutty, N., A. T. Evan, C. Monfreda, and J. A. Foley, 2008: Farming the planet: 1. geographic distribution of global agricultural lands in the year 2000. *Global biogeochemical cycles*, **22 (1)**.

Rohde, R., and Coauthors, 2013: Berkeley earth temperature averaging process. *Geoinformatics & Geostatistics: An Overview*, **1 (2)**, 1–13.

Sacks, W. J., D. Deryng, J. A. Foley, and N. Ramankutty, 2010: Crop planting dates: an analysis of global patterns. *Global Ecology and Biogeography*, **19 (5)**, 607–620.

Sánchez, B., A. Rasmussen, and J. R. Porter, 2014: Temperatures and the growth and development of maize and rice: a review. *Global change biology*, **20 (2)**, 408–417.

Schlenker, W., and M. J. Roberts, 2009: Nonlinear temperature effects indicate severe damages to us crop yields under climate change. *Proceedings of the National Academy of sciences*, **106 (37)**, 15 594–15 598.

Troy, T. J., C. Kipgen, and I. Pal, 2015: The impact of climate extremes and irrigation on us crop yields. *Environmental Research Letters*, **10 (5)**, 054 013.

Valadão, C. E., L. M. Carvalho, P. S. Lucio, and R. R. Chaves, 2017: Impacts of the madden-julian oscillation on intraseasonal precipitation over northeast brazil. *International Journal of Climatology*, **37 (4)**, 1859–1884.

Vigaud, N., and A. Giannini, 2018: West african convection regimes and their predictability from submonthly forecasts. *Climate Dynamics*, 1–20.

Vitart, F., and A. W. Robertson, 2018: The sub-seasonal to seasonal prediction project (s2s) and the prediction of extreme events. *npj Climate and Atmospheric Science*, **1 (1)**, 3.

Wheeler, M. C., and H. H. Hendon, 2004: An all-season real-time multivariate mjo index: Development of an index for monitoring and prediction. *Monthly Weather Review*, **132 (8)**, 1917–1932.

Wheeler, M. C., H. H. Hendon, S. Cleland, H. Meinke, and A. Donald, 2009: Impacts of the madden–julian oscillation on australian rainfall and circulation. *Journal of Climate*, **22 (6)**, 1482–1498.

White, C. J., and Coauthors, 2017: Potential applications of subseasonal-to-seasonal (s2s) predictions. *Meteorological applications*, **24 (3)**, 315–325.

Wilks, D. S., 2016: "the stippling shows statistically significant gridpoints": How research results are routinely overstated and over-interpreted, and what to do about it. *Bulletin of the American Meteorological Society*, **(2016)**.

Zhang, C., 2005: Madden-julian oscillation. *Reviews of Geophysics*, **43 (2)**.

Zhang, C., and M. Dong, 2004: Seasonality in the madden–julian oscillation. *Journal of climate*, **17 (16)**, 3169–3180.

Zhou, S., M. L'Heureux, S. Weaver, and A. Kumar, 2012: A composite study of the mjo influence on the surface air temperature and precipitation over the continental united states. *Climate dynamics*, **38 (7-8)**, 1459–1471.

List of Figures

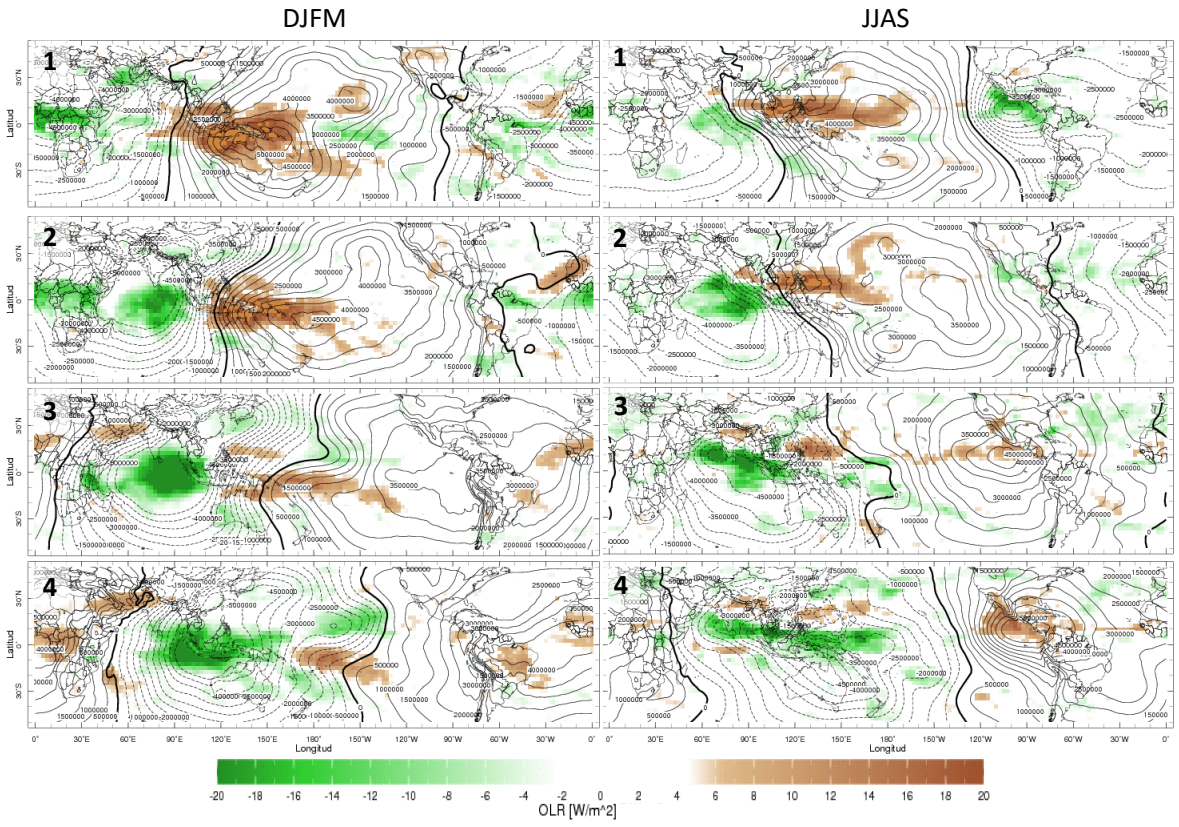

Figure 1. MJO convection anomalies in phases 1-4 during Dec-Mar (left column) and Jun-Sep (right column). Outgoing longwave radiation (OLR; colors) and 200 hPa vertical velocity potential (contours) for phases 1-4 (left panels) and phases 5-8 (right panels). Negative OLR indicates increased cloud cover, which is often an indication of increased precipitation. Positive OLR indicates clear sky conditions associated with atmospheric descent and dry conditions. A negative velocity potential at 200 hPa indicates divergence in the upper atmosphere, which is caused by deep convection in the region, while a positive velocity potential indicates a stable upper atmosphere. User-specified seasonal composites available in IRI Data Library MJO Maproom: *http://iridl.ldeo.columbia.edu/maproom/Global/Climatologies/MJO_SPH.html*

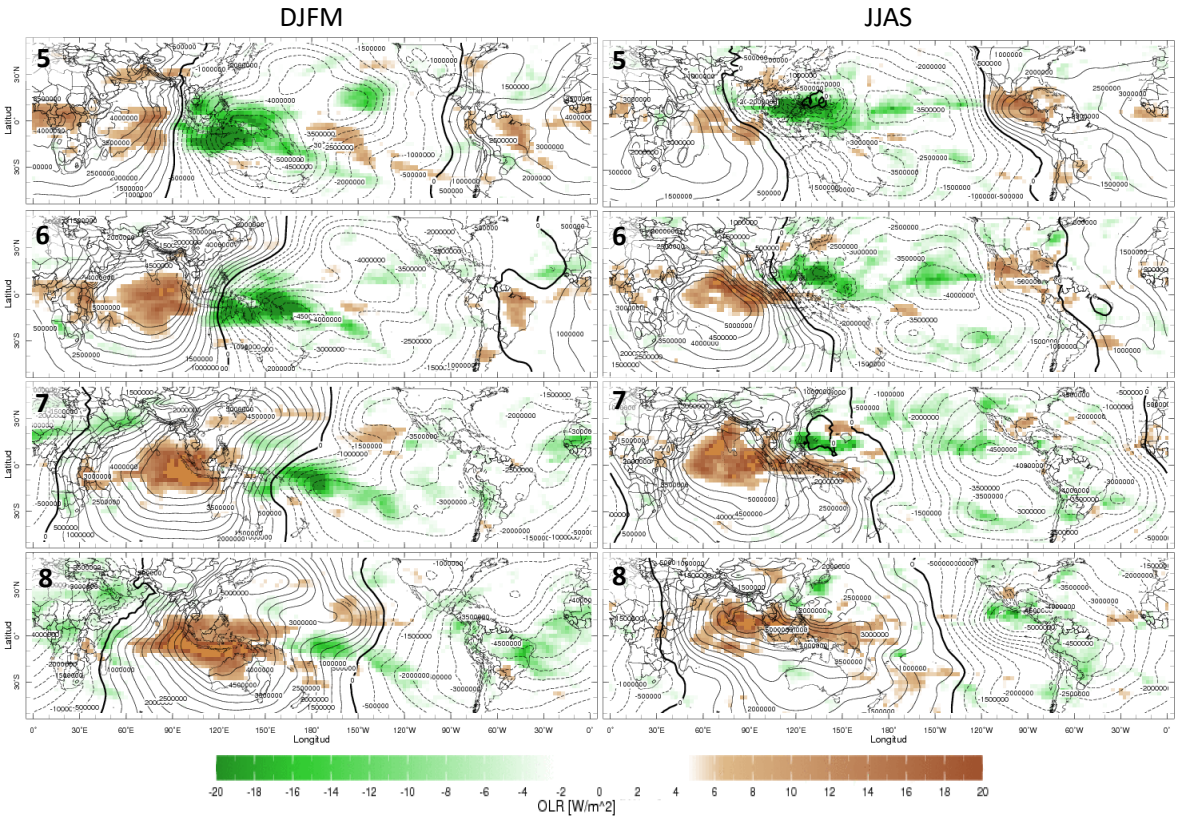

Figure 2. MJO convection anomalies in phases 5-8 during Dec-Mar (left column) and Jun-Sep (right column). Outgoing longwave radiation (colors) and 200 hPa vertical velocity potential (contours) for phases 1-4 (left panels) and phases 5-8 (right panels). Negative OLR indicates increased cloud cover, which is often an indication of increased precipitation. Positive OLR indicates clear sky conditions associated with atmospheric descent and dry conditions. A negative velocity potential at 200 hPa indicates divergence in the upper atmosphere, which is caused by deep convection in the region, while a positive velocity potential indicates a stable upper atmosphere. User-specified seasonal composites available in IRI Data Library MJO Maproom: *http://iridl.ldeo.columbia.edu/maproom/Global/Climatologies/MJO_SPH.html*

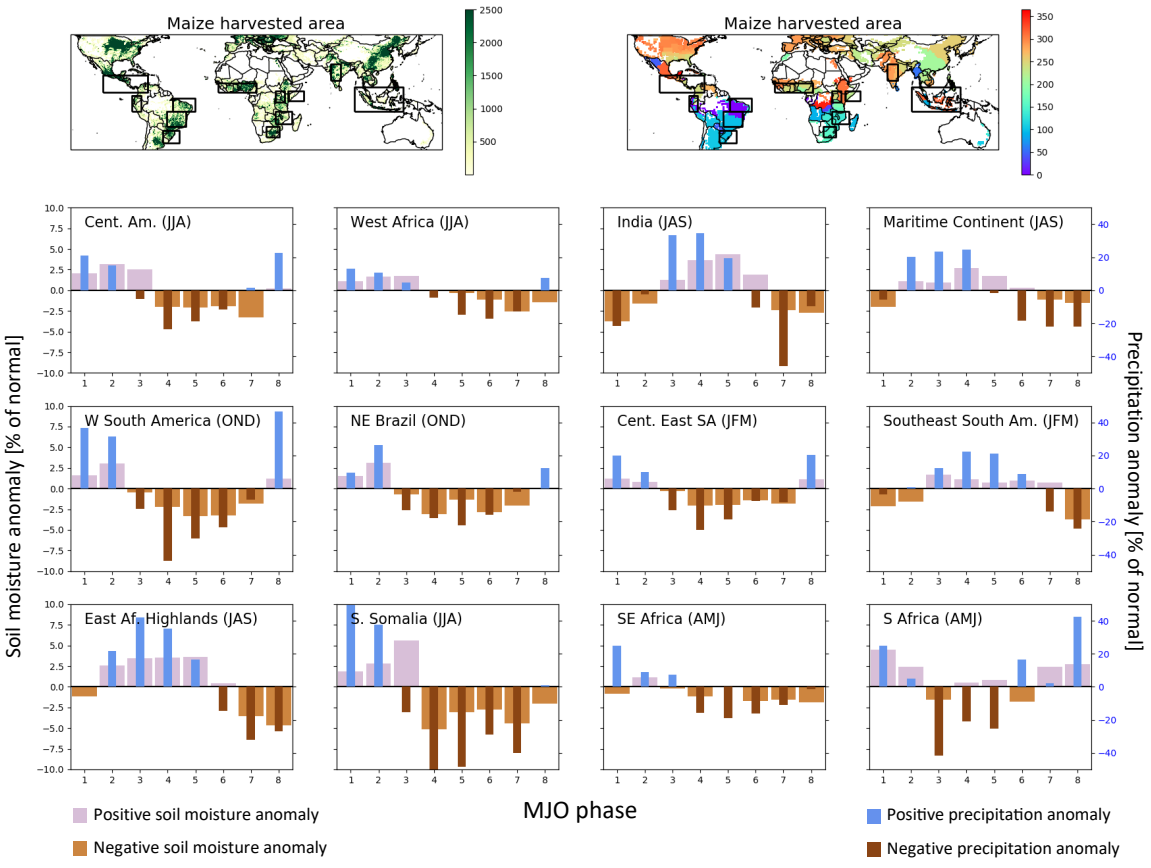

Figure 3. Relative strength of MJO teleconnections during the maize growing season. Top row: number of phases with statistically significant ($p<0.05$) precipitation (left panel) and soil moisture (right panel) teleconnections. Bottom three rows: Precipitation (thin blue and brown bars) and soil moisture (thick purple and brown bars) anomalies during each MJO phase relative to an average day when MJO is inactive during the growing season. Regions defined by boxes shown in the top row. A precipitation bar in a given phase with a value of 20%, for example, indicates that on average precipitation during that phase is 20% greater compared to an average day in the growing season when the MJO is inactive.

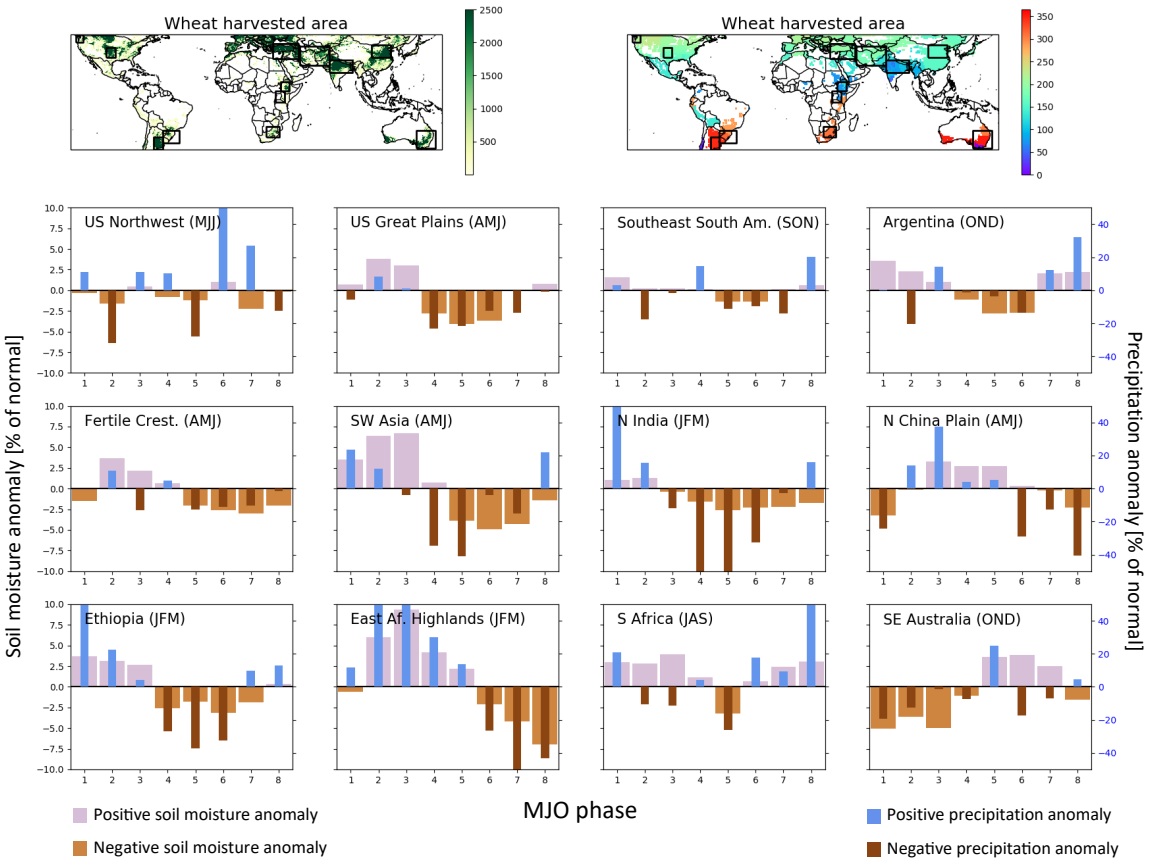

Figure 4. Relative strength of MJO teleconnections during the wheat growing season. Top row: number of phases with statistically significant ($p<0.05$) precipitation (left panel) and soil moisture (right panel) teleconnections. Bottom three rows: Precipitation (thin blue and brown bars) and soil moisture (thick purple and brown bars) anomalies during each MJO phase relative to an average day when MJO is inactive during the growing season. Regions defined by boxes shown in the top row. A precipitation bar in a given phase with a value of 20%, for example, indicates that on average precipitation during that phase is 20% greater compared to an average day in the growing season when the MJO is inactive.

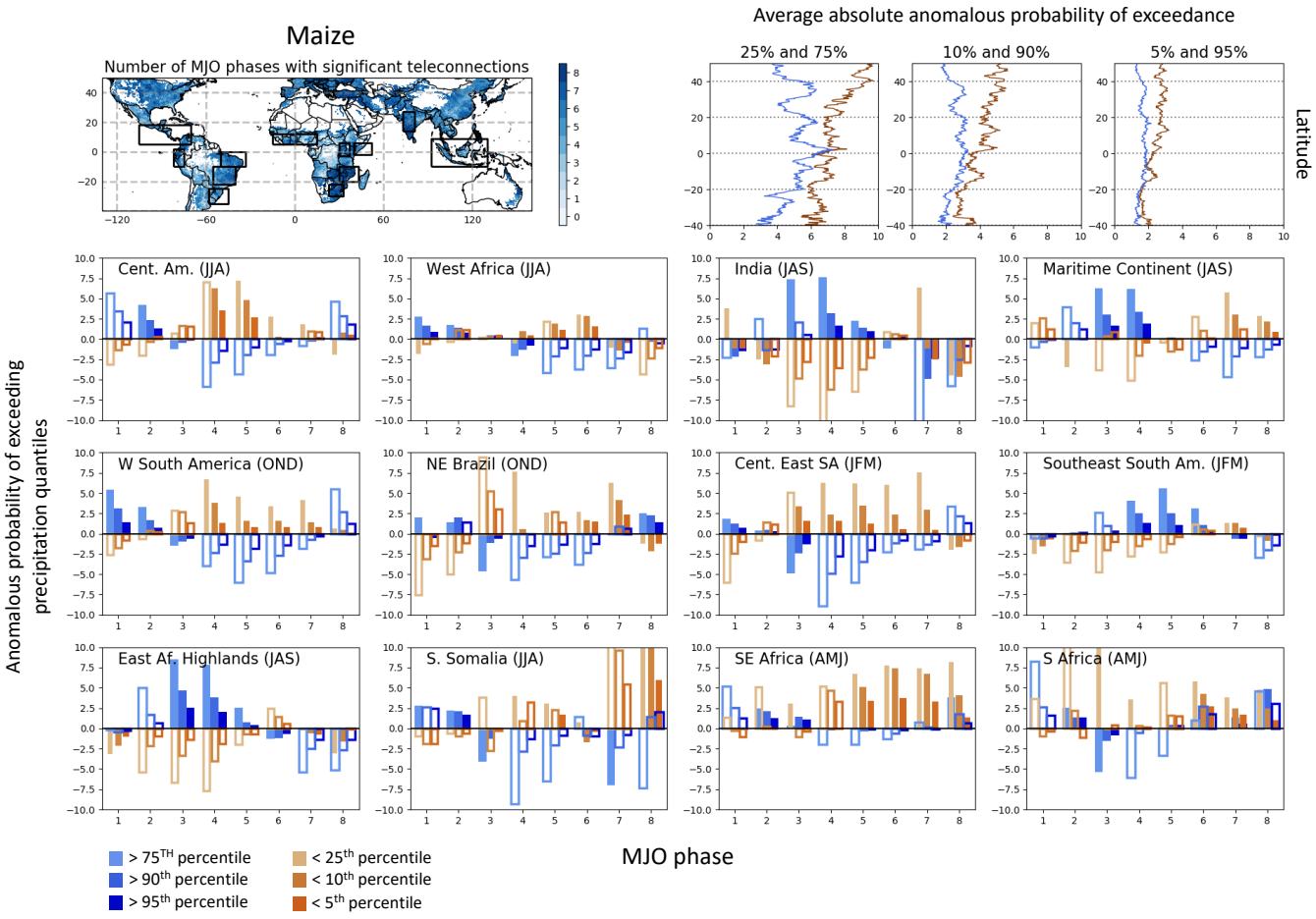

718 Figure 5. MJO effects on the probability of a region experiencing moderate or extreme precipitation events
719 during the maize growing season. Top row: number of MJO phases with statistically significant ($p<0.05$)
720 precipitation teleconnections (left panel), absolute changes in the probability of dry (brown line) or wet (blue
721 line) events during an active MJO, averaged over all grid cells in a latitude (right three panels; event percentiles
722 in panel labels). Bottom three rows: MJO effects on the probability of exceeding the 75% (light blue), 90%
723 (medium blue), or 95% (dark blue) threshold for daily precipitation, or for negatively exceeding the 25% (light
724 brown), 10% (medium brown), or 5% (dark brown) threshold by MJO phase for each region shown in the top left
725 plot. A light brown bar (25th percentile event) with a height of 5% during a given phase, for example, indicates
726 that an event at least as dry as the 25th percentile event happens in 30% of the days when the MJO is in that
727 phase. Solid bars are statistically significant at the 95% confidence level.

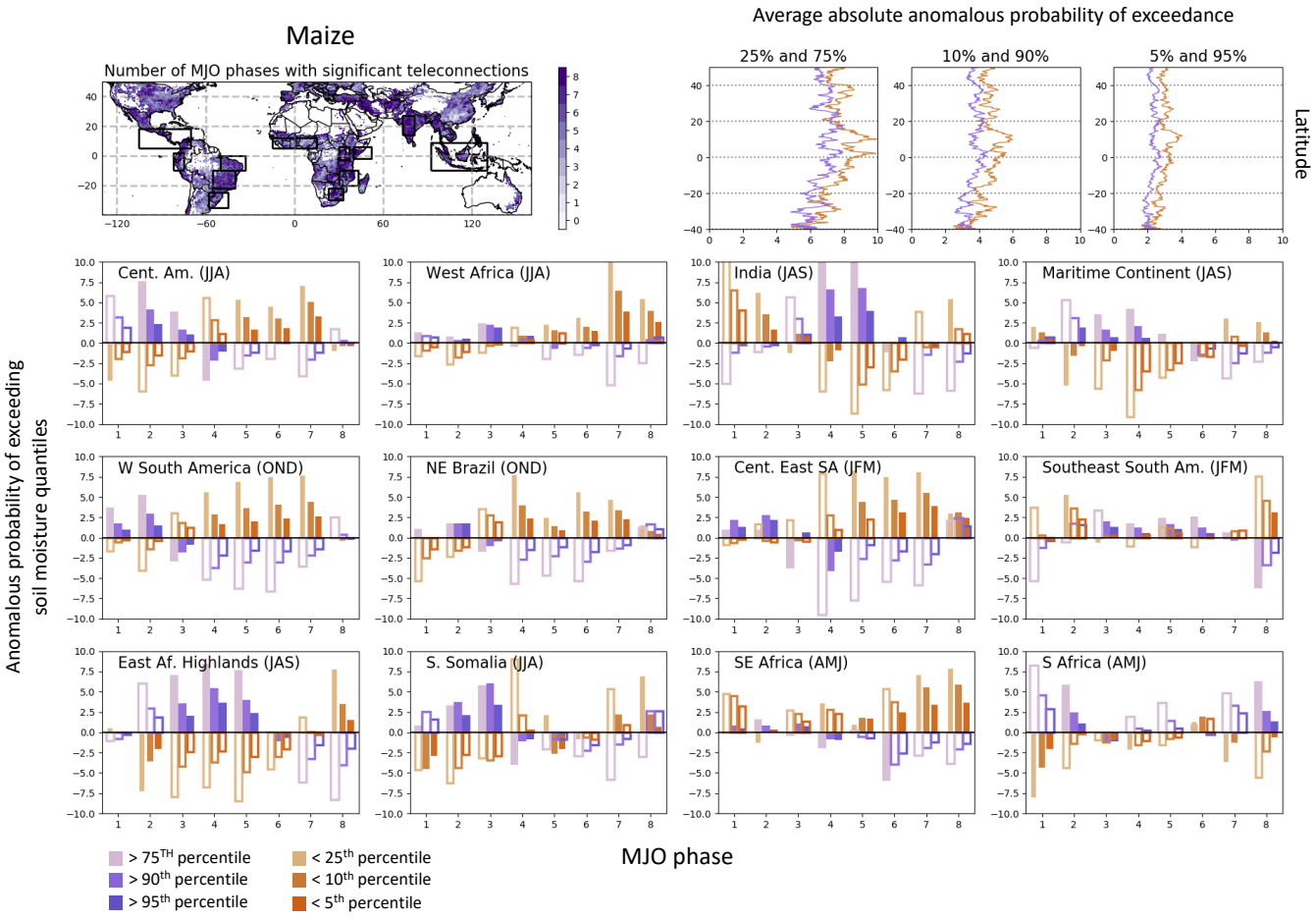

Figure 6. MJO effects on the probability of a region experiencing moderate or extreme soil moisture events during the maize growing season. Top row: number of MJO phases with statistically significant ($p<0.05$) soil moisture teleconnections (left panel), absolute changes in the probability of dry (brown line) or wet (purple line) events during an active MJO, averaged over all grid cells in a latitude (right three panels; event percentiles in panel labels). Bottom three rows: MJO effects on the probability of exceeding the 75% (light purple), 90% (medium purple), or 95% (dark purple) threshold for daily precipitation, or for negatively exceeding the 25% (light brown), 10% (medium brown), or 5% (dark brown) threshold by MJO phase for each region shown in the top left plot. A light brown bar (25th percentile event) with a height of 5% during a given phase, for example, indicates that an event at least as dry as the 25th percentile event happens in 30% of the days when the MJO is in that phase. Solid bars are statistically significant at the 95% confidence level.

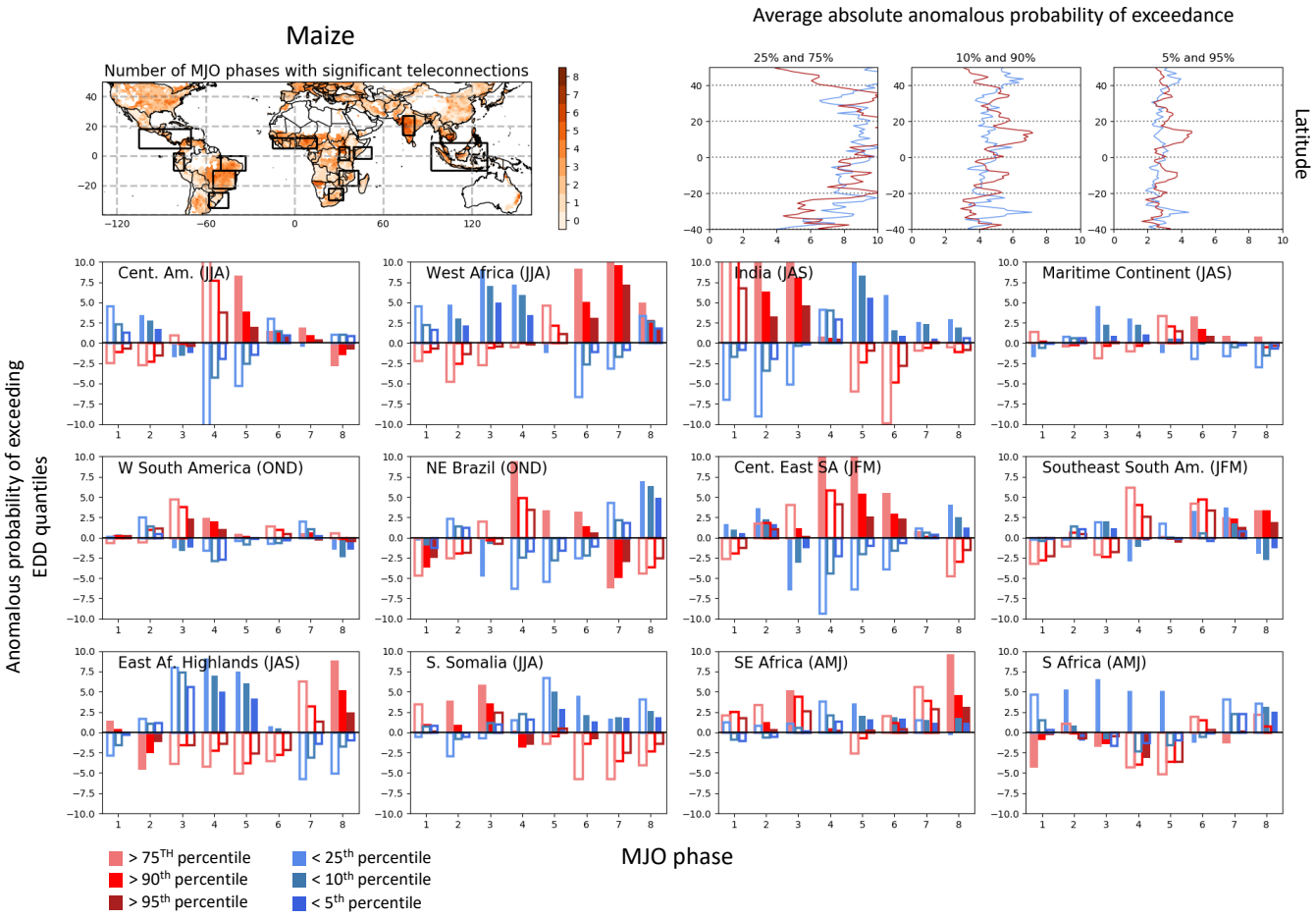

738 Figure 7. MJO effects on the probability of a region experiencing moderate or extreme maximum temperature
739 events during the maize growing season. Top row: number of MJO phases with statistically significant ($p<0.05$)
740 maximum temperature teleconnections (left panel), absolute changes in the probability of hot (red line) or cool
741 (blue line) events during an active MJO, averaged over all grid cells in a latitude (right three panels; event
742 percentiles in panel labels). Bottom three rows: MJO effects on the probability of exceeding the 75% (light
743 red), 90% (medium red), or 95% (dark red) threshold for daily precipitation, or for negatively exceeding the
744 25% (light blue), 10% (medium blue), or 5% (dark blue) threshold by MJO phase for each region shown in the
745 top left plot. A light blue bar (25th percentile event) with a height of 5% during a given phase, for example,
746 indicates that an event at least as cool as the 25th percentile event happens in 30% of the days when the MJO is
747 in that phase. Solid bars are statistically significant at the 95% confidence level.

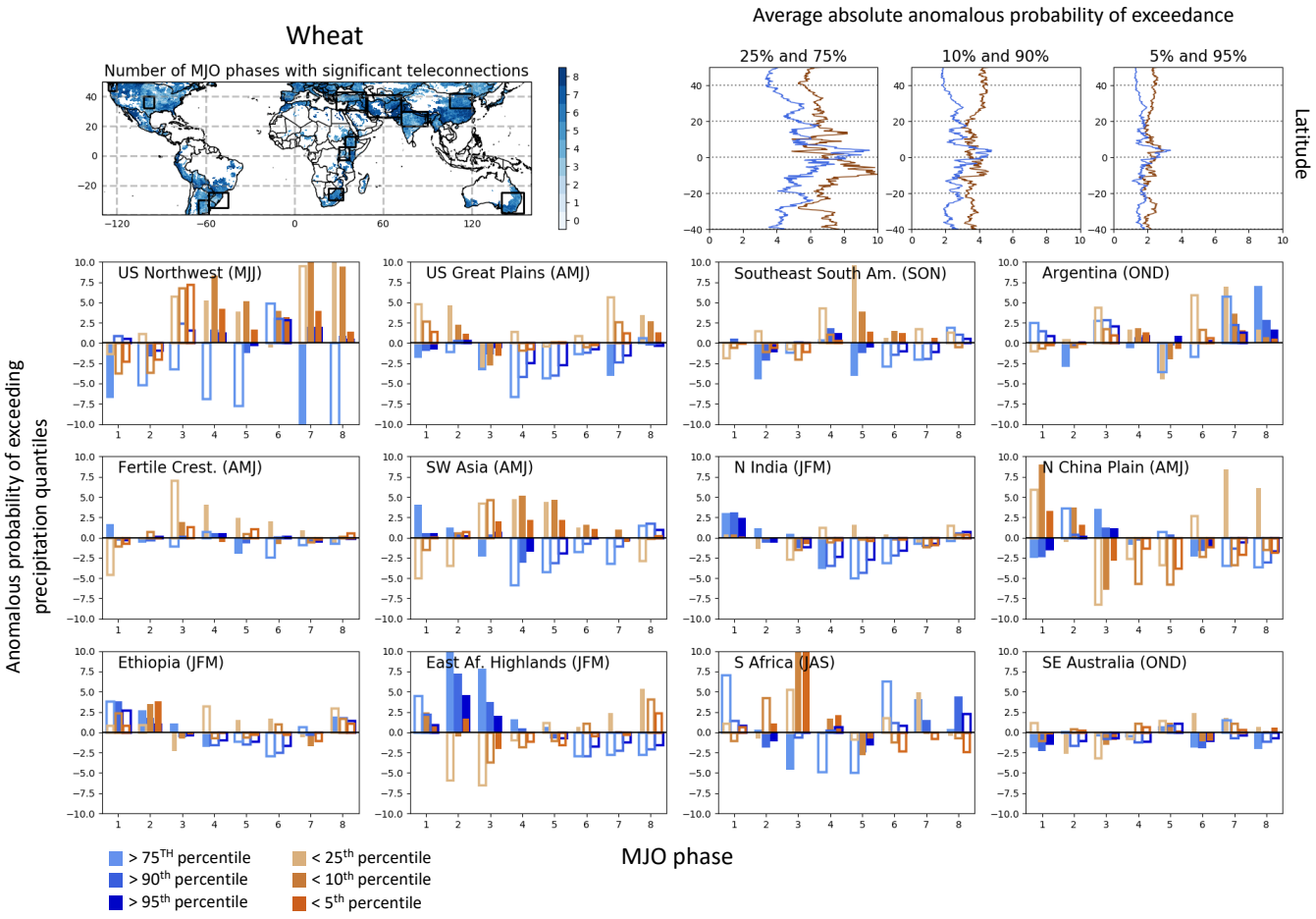

Figure 8. MJO effects on the probability of a region experiencing moderate or extreme precipitation events during the wheat growing season. Top row: number of MJO phases with statistically significant ($p<0.05$) precipitation teleconnections (left panel), absolute changes in the probability of dry (brown line) or wet (blue line) events during an active MJO, averaged over all grid cells in a latitude (right three panels; event percentiles in panel labels). Bottom three rows: MJO effects on the probability of exceeding the 75% (light blue), 90% (medium blue), or 95% (dark blue) threshold for daily precipitation, or for negatively exceeding the 25% (light brown), 10% (medium brown), or 5% (dark brown) threshold by MJO phase for each region shown in the top left plot. A light brown bar (25th percentile event) with a height of 5% during a given phase, for example, indicates that an event at least as dry as the 25th percentile event happens in 30% of the days when the MJO is in that phase. Solid bars are statistically significant at the 95% confidence level.

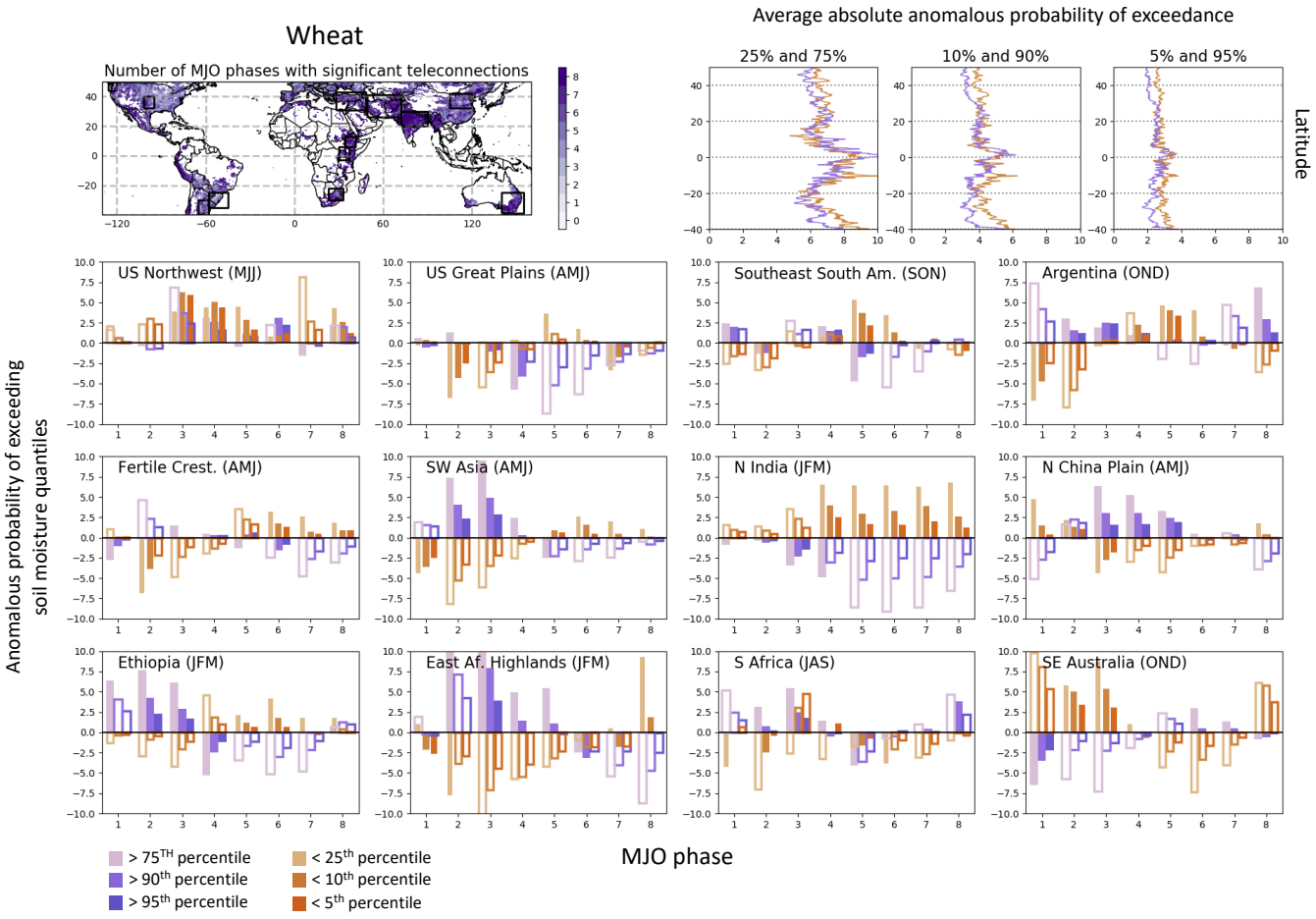

Figure 9. MJO effects on the probability of a region experiencing moderate or extreme soil moisture events during the wheat growing season. Top row: number of MJO phases with statistically significant ($p<0.05$) soil moisture teleconnections (left panel), absolute changes in the probability of dry (brown line) or wet (blue line) events during an active MJO, averaged over all grid cells in a latitude (right three panels; event percentiles in panel labels). Bottom three rows: MJO effects on the probability of exceeding the 75% (light purple), 90% (medium purple), or 95% (dark purple) threshold for daily precipitation, or for negatively exceeding the 25% (light brown), 10% (medium brown), or 5% (dark brown) threshold by MJO phase for each region shown in the top left plot. A light brown bar (25th percentile event) with a height of 5% during a given phase, for example, indicates that an event at least as dry as the 25th percentile event happens in 30% of the days when the MJO is in that phase. Solid bars are statistically significant at the 95% confidence level.

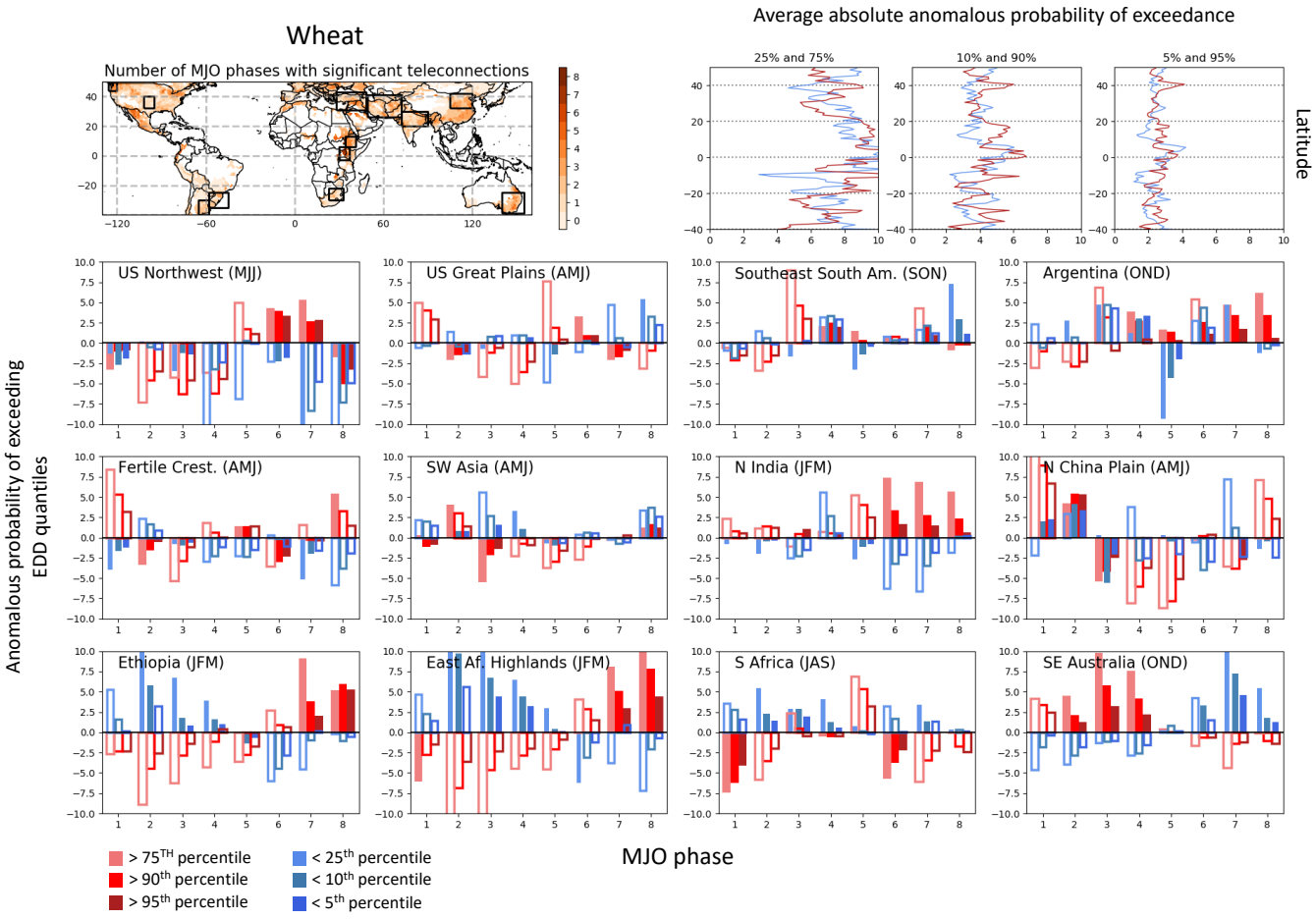

Figure 10. MJO effects on the probability of a region experiencing moderate or extreme maximum temperature events during the wheat growing season. Top row: number of MJO phases with statistically significant ($p<0.05$) maximum temperature teleconnections (left panel), absolute changes in the probability of hot (red line) or cool (blue line) events during an active MJO, averaged over all grid cells in a latitude (right three panels; event percentiles in panel labels). Bottom three rows: MJO effects on the probability of exceeding the 75% (light red), 90% (medium red), or 95% (dark red) threshold for daily precipitation, or for negatively exceeding the 25% (light blue), 10% (medium blue), or 5% (dark blue) threshold by MJO phase for each region shown in the top left plot. A light blue bar (25th percentile event) with a height of 5% during a given phase, for example, indicates that an event at least as cool as the 25th percentile event happens in 30% of the days when the MJO is in that phase. Solid bars are statistically significant at the 95% confidence level.

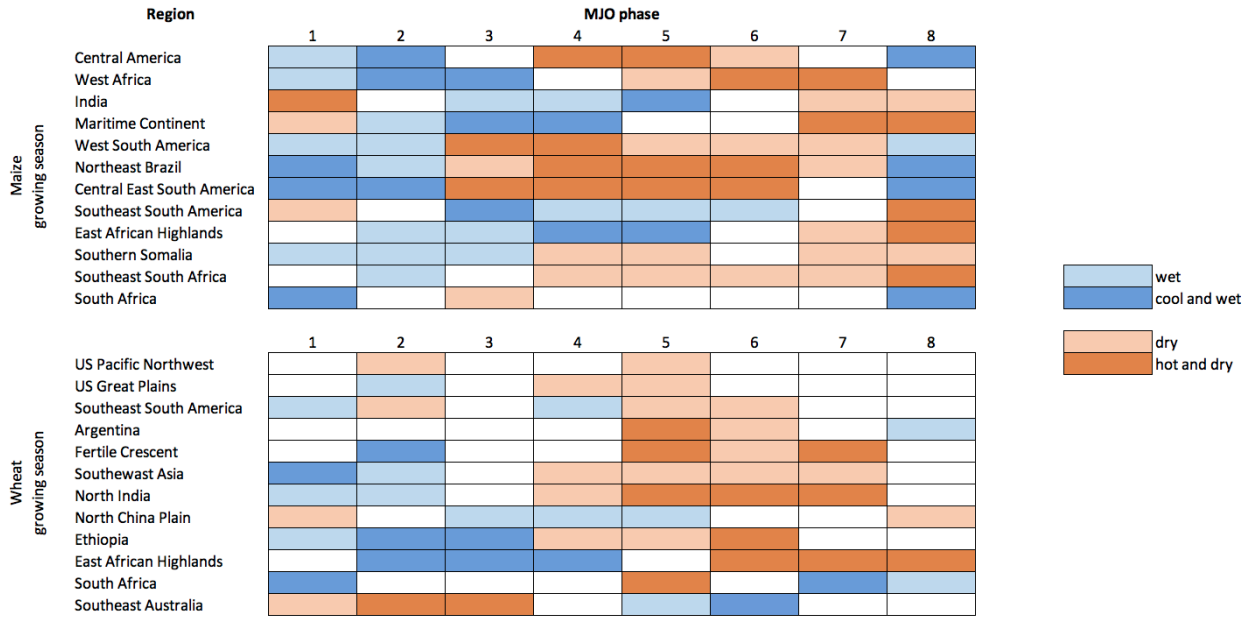

778 Figure 11. Summary of MJO teleconnections to maize and wheat growing seasons by region. See Figures 3 -
779 10 for region locations and quantitative analysis of growing season teleconnections.

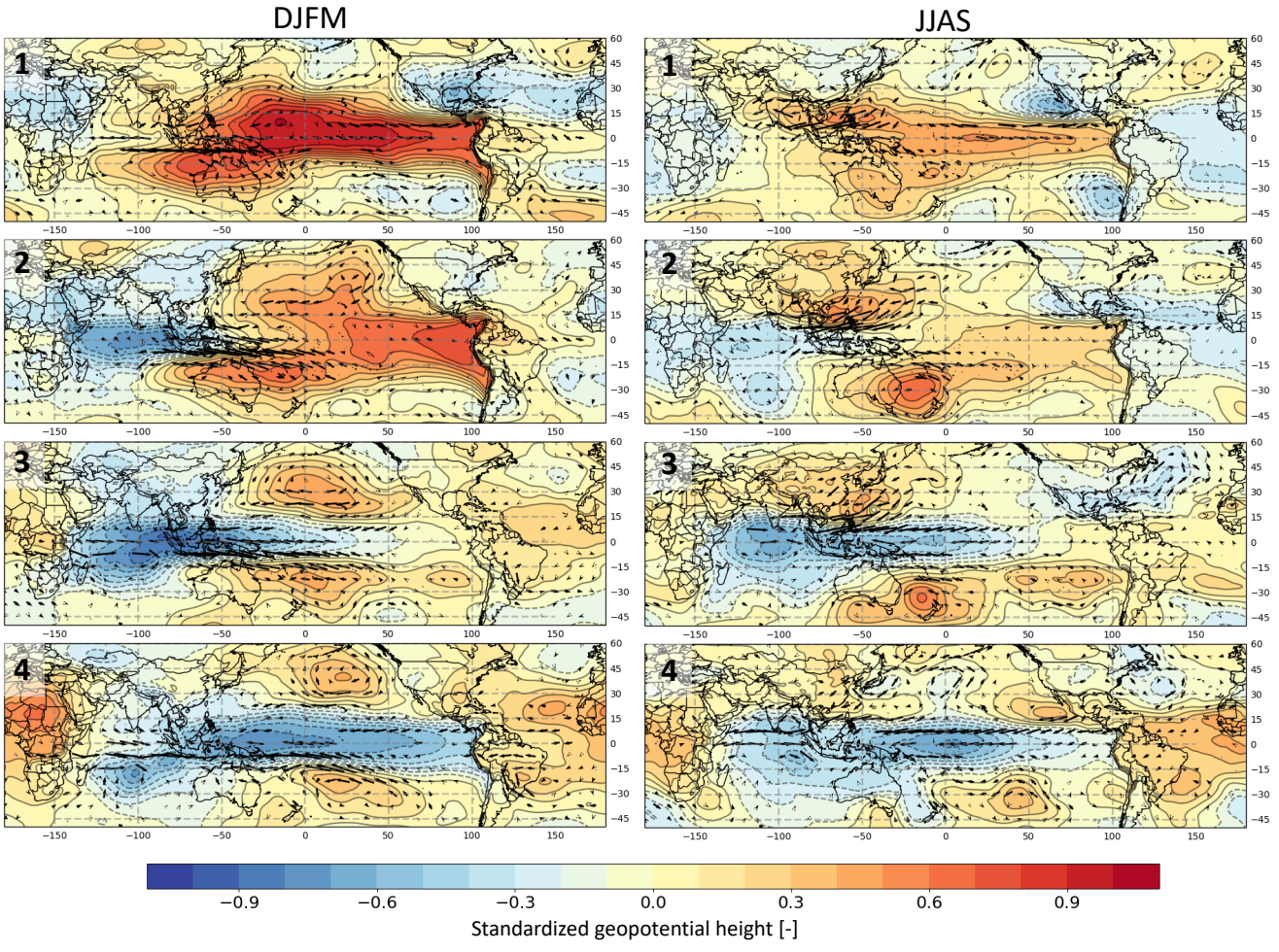

Figure 12. MJO atmospheric teleconnections in phases 1-4 during Dec-Mar (left column) and Jun-Sep (right column). Colors and contours indicate standardized 850hPa geopotential height anomalies during each phase of the MJO. Arrows indicate vertically integrated moisture flux. User-specified seasonal composites available in IRI Data Library MJO Maproom: *http://iridl.ldeo.columbia.edu/maproom/Global/Climatologies/MJO_SPH.html*

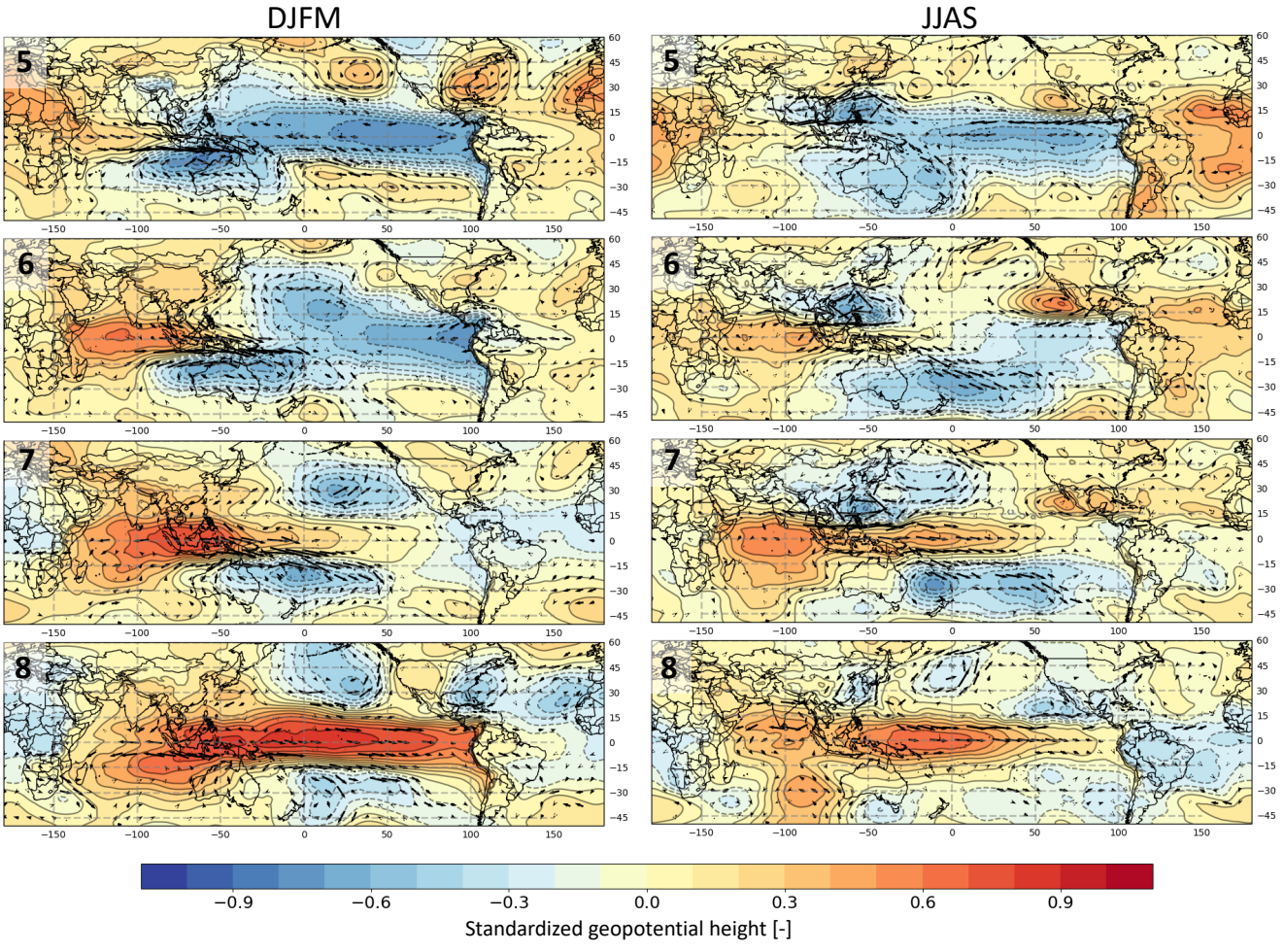

Figure 13. MJO atmospheric teleconnections in phases 5-8 during Dec-Mar (left column) and Jun-Sep (right column). Colors and contours indicate standardized 850hPa geopotential height anomalies during each phase of the MJO. Arrows indicate vertically integrated moisture flux. User-specified seasonal composites available in IRI Data Library MJO Maproom: *http://iridl.ldeo.columbia.edu/maproom/Global/Climatologies/MJO_SPH.html*